

Long-range magnetic order in the $5d^2$ double perovskite $\text{Ba}_2\text{CaOsO}_6$: Comparison with spin-disordered Ba_2YReO_6

C M Thompson^{1,2}, J P Carlo³, R Flacau⁴, T Aharen^{1,5},
I A Leahy³, J R Pollicemi³, T J S Munsie⁶, T Medina⁶,
G M Luke^{6,2,7}, J Munevar⁸, S Cheung⁹, T Goko⁹,
Y J Uemura⁹ and J E Greedan^{1,2}

¹Department of Chemistry and Chemical Biology, McMaster University,
Hamilton, ON L8S 4M1, Canada

²Brockhouse Institute for Materials Research, McMaster University, Hamilton,
ON L8S 4M1 Canada

³Department of Physics, Villanova University, Villanova, PA 19085 USA

⁴Canadian Neutron Beam Centre, Chalk River Laboratories, Chalk River, ON
K0J 1J0, Canada

⁵Department of Energy and Hydrocarbon Chemistry, Graduate School of
Engineering, Kyoto University, Nishikyo-Ku, Kyoto 615-8510, Japan

⁶Department of Physics and Astronomy, McMaster University, Hamilton, ON
L8S 4M1, Canada

⁷Canadian Institute For Advanced Research, Toronto, ON, M5G 1Z8 Canada

⁸Centro Brasileiro Pesquisas Fisicas (CBPF), Rio de Janeiro, Brazil

⁹Department of Physics, Columbia University, New York, NY 10027 USA

E-mail: jeremy.carlo@villanova.edu

Abstract. The B-site ordered double perovskite $\text{Ba}_2\text{CaOsO}_6$ was studied by d.c. magnetic susceptibility, powder neutron diffraction and muon spin relaxation methods. The lattice parameter is $a = 8.3619(6)$ Å at 280 K and cubic symmetry ($Fm\bar{3}m$) is retained to 3.5 K with $a = 8.3462(7)$ Å. Curie-Weiss susceptibility behaviour is observed for $T > 100$ K and the derived constants are $C = 0.3361(3)$ emu-K/mole and $\Theta_{CW} = -156.2(3)$ K, in excellent agreement with literature values. This Curie constant is much smaller than the spin-only value of 1.00 emu-K/mole for a $5d^2$ Os^{6+} configuration, indicating a major influence of spin-orbit coupling. Previous studies had detected both susceptibility and heat capacity anomalies near 50 K but no definitive conclusion was drawn concerning the nature of the ground state. While no ordered Os moment could be detected by powder neutron diffraction, muon spin relaxation (μSR) data show clear long-lived oscillations indicative of a continuous transition to long-range magnetic order below $T_C = 50$ K. An estimate of the ordered moment on Os^{6+} is $\sim 0.2 \mu_B$, based upon a comparison with μSR data for Ba_2YRuO_6 with a known ordered moment of $2.2 \mu_B$. These results are compared with those for isostructural Ba_2YReO_6 which contains Re^{5+} , also $5d^2$, and has a nearly identical unit cell constant, $a = 8.36278(2)$ Å – a structural doppelgänger. In contrast, Ba_2YReO_6 shows $\Theta_{CW} = -616$ K, and a complex spin-disordered and, ultimately, spin-frozen ground state below 50 K, indicating a much higher level of geometric frustration than in $\text{Ba}_2\text{CaOsO}_6$. The results on these $5d^2$ systems are compared to recent theory, which predicts a variety of ferromagnetic and antiferromagnetic ground states. In the case of $\text{Ba}_2\text{CaOsO}_6$, our data indicate that a complex four-sublattice magnetic structure is likely. This is in contrast to the spin-disordered ground state in Ba_2YReO_6 , despite a lack of evidence for structural disorder, for which theory currently provides no clear explanation.

PACS numbers: 75.25.-j, 75.10.Jm, 75.40.Cx, 75.47.Lx, 75.50.-y, 75.70.Tj,
76.75.+i

1. Introduction

Oxides with the double perovskite structure with rock-salt ordering of B cations [1] provide many opportunities for the design of new materials with the potential to exhibit geometric magnetic frustration. Such materials have the general composition $A_2BB'O_6$, where A is a large cation such as the divalent ions from Group 2 (Ca, Sr or Ba) or trivalent ions from Group 3 (La and other large rare earth ions) and B and B' typically are smaller cations from the $3d$, $4d$ and $5d$ transition series in a variety of oxidation states and electronic configurations but can include smaller ions from Groups 2 and 3 such as Mg and Ca. Geometric magnetic frustration can arise when B is a diamagnetic ion and B' is magnetic as these sites are crystallographically distinct and each forms a face-centered cubic sublattice, which is equivalent to a network of edge-sharing tetrahedra as shown in Figure 1. In the presence of antiferromagnetic nearest-neighbor correlations between B' cations such a lattice exhibits frustration.

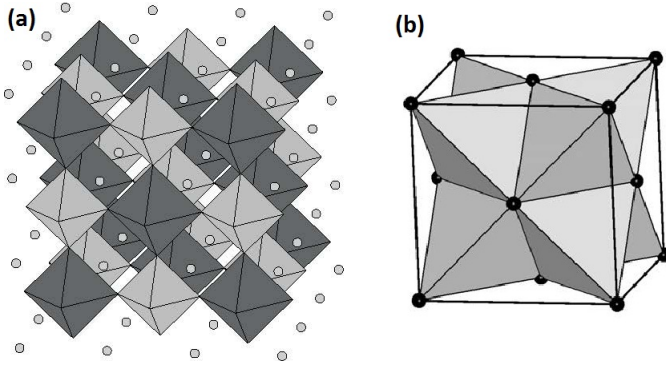


Figure 1. (a) The crystal structure of the B-site ordered double perovskite, $A_2BB'O_6$. The grey spheres, light grey octahedra and dark grey octahedra represent A ions, BO_6 octahedra and $B'O_6$ octahedra, respectively. (b) The geometrically frustrated face-centered-cubic lattice of edge-sharing tetrahedra formed by the B' sites.

The symmetry of the B' sublattice and the local point symmetry at the B' ion site are determined by Goldschmidt's tolerance factor,

$$t = (A - O) / \sqrt{2}(< B, B' > - O) \quad (1)$$

where $A-O$ and $< B, B' > - O$ are the relevant cation – oxide ion distances [2]. As t decreases from the ideal value of 1, space group symmetries $Fm\bar{3}m$, $I4/m$ and $P2_1/n$ are observed sequentially, with respective B' site point symmetries of $m\bar{3}m$, $4/m$ and $\bar{1}$ [3]. The point symmetries determine the crystal field splitting of the t_{2g}^n ground states. Of course the B' site electronic configuration confers a nominal spin, S , which can be strongly modified by the magnitude of the single ion spin orbit coupling (SOC) constant λ . All of these factors – sublattice symmetry, point symmetry, S and SOC – are degrees of freedom which can play a role in the determination of the magnetic ground state. Recent theory has attempted to take these factors into account at the mean field level [4, 5, 6].

In Table I some results for known double perovskites are catalogued. Some trends are evident. For $S > 1$, antiferromagnetic long range order (AFLRO) is almost always found. The frustration indices, defined as $f = |\Theta_{CW}|/T_{\text{order}}$, vary widely from 3

to 16. In some cases, for example Ba_2YRuO_6 , there are anomalies. This material shows two susceptibility maxima and an unexpected gap of ~ 5 meV in the inelastic neutron spectrum at $|Q| = 0.76 \text{ \AA}^{-1}$, the location of the (100) magnetic reflection. The presence of the gap has been attributed to the influence of SOC [7, 8]. It is not known whether a similar feature exists for monoclinic $\text{La}_2\text{LiRuO}_6$. For $S = 1$, AFLRO seems rare, being known only when B' is the $3d$ ion, Ni^{2+} [9]. The two cases with nominal $S = 1$ for the $5d$ ion, Re^{5+} , both show quite complex magnetic behaviour which has in the case of Ba_2YReO_6 been characterized by two distinct spin relaxation processes which lead ultimately to a spin-frozen ground state [10]. $\text{La}_2\text{LiReO}_6$ seems to feature a singlet ground state which remains poorly understood [10]. For systems with nominal $S = 1/2$ a great variety of behaviours and ground states are observed including both ferromagnetic and antiferromagnetic long range order with minimal frustration for two materials involving Os^{7+} , $\text{Ba}_2\text{NaOsO}_6$ and $\text{Ba}_2\text{LiOsO}_6$ [11, 12, 13]. In contrast, Ba_2YMoO_6 exhibits the same $Fm\bar{3}m$ symmetry but its ground state is a unique, gapped singlet with $f > 100$ [14, 15, 16]. Upon lowering the symmetry to $P2_1/n$ in $\text{La}_2\text{LiMoO}_6$, both the high frustration and the singlet state disappear and a more ordered ground state emerges [15].

Table 1. Comparison of frustrated double perovskite systems. *This is the nominal spin quantum number assuming L–S coupling. For $4d$ and $5d$ ions with $S = 1$ and $1/2$ spin-orbit coupling will add a significant orbital contribution which cannot be ignored. **This is the frustration index, $f = |\Theta_{CW}|/T_{cf}$. T_{cf} refers to the temperature below which either long range order, T_c , or apparent spin freezing, T_f , occurs. B' symm. refers to the point group symmetry at the magnetic B' site. AFLRO and FLRO refer to antiferromagnetic and ferromagnetic long range order. INC refers to long range incommensurate magnetic order, and SRINC to short range incommensurate order. AFSRO signals short range antiferromagnetic order. SF (spin frozen) indicates a non-LRO ground state in which static spins have been detected. SING? indicates a singlet ground state as yet not well characterized. GSING refers to a gapped singlet ground state. λ is the estimated single-ion SOC constant for the magnetic ion in question.

S^*	Compound	Θ_{CW} (K)	T_{cf} (K)	f^{**}	B' symm.	Ground State	λ (meV)	Reference
5/2	Ba_2MnWO_6	−64	7.5	9	$m\bar{3}m$	AFLRO	—	[17, 18]
5/2	Sr_2MnWO_6	−71	14	5	$\bar{1}$	AFLRO	—	[18, 19]
3/2	Ba_2YRuO_6	−571	36	16	$m\bar{3}m$	AFLRO	200	[7]
3/2	$\text{La}_2\text{LiRuO}_6$	−170	23.8	7	$\bar{1}$	AFLRO	200	[7]
3/2	$\text{La}_2\text{NaRuO}_6$	−57	15	4	$\bar{1}$	INC	200	[20, 21]
3/2	$\text{La}_2\text{NaOsO}_6$	−74	12	6	$\bar{1}$	SRINC	630	[20, 21]
1	Sr_2NiWO_6	−175	54	3	$4/m$	AFLRO	40	[9]
1	Ba_2YReO_6	−616	35	18	$m\bar{3}m$	SF	590	[10]
1	$\text{La}_2\text{LiReO}_6$	−204	?	?	$\bar{1}$	SING?	590	[10]
1/2	$\text{Ba}_2\text{LiOsO}_6$	−40	8	5	$m\bar{3}m$	AFLRO	630	[11]
1/2	$\text{Ba}_2\text{NaOsO}_6$	−10	6.8	~ 1	$m\bar{3}m$	FLRO	630	[11]
1/2	Ba_2YMoO_6	−219	<2	>400	$m\bar{3}m$	GSING	135	[15]
1/2	$\text{La}_2\text{LiMoO}_6$	−45	4?	11	$\bar{1}$	AFSRO	135	[15]
1/2	$\text{Sr}_2\text{CaReO}_6$	−443	14	32	$\bar{1}$	SF	590	[22]
1/2	$\text{Sr}_2\text{MgReO}_6$	−426	45	9	$\bar{1}$	SF	590	[23]

In order to investigate further the possible systematics among this family of double

perovskites, the material $\text{Ba}_2\text{CaOsO}_6$, containing $5d^2 \text{Os}^{6+}$, which is isoelectronic with Re^{5+} , has been studied in detail. This compound has been reported to crystallize in $Fm\bar{3}m$, a symmetry which is retained to 17 K according to x-ray diffraction results [24]. There is a remarkable accord in unit cell constant ($a = 8.359(5) \text{ \AA}$) with that for Ba_2YReO_6 ($a = 8.36278(2) \text{ \AA}$), and the importance of SOC should be very similar, making this material a true doppelgänger to Ba_2YReO_6 . Heat capacity and susceptibility data indicate an anomaly near 50 K but no firm conclusion was drawn concerning the nature of the ground state [24]. Ba_2YReO_6 shows similar maxima in susceptibility and heat capacity at 25 K and 50 K [10]. In this study the results of magnetic susceptibility, neutron powder diffraction and muon spin relaxation experiments are described and conclusions drawn regarding the nature of the ground state in $\text{Ba}_2\text{CaOsO}_6$. Both materials are discussed in the context of recent theory on double perovskites [4, 5, 6].

2. Experimental

2.1. Sample Preparation

$\text{Ba}_2\text{CaOsO}_6$ was prepared by a conventional solid state reaction. Stoichiometric amounts of BaO_2 , CaO , and Os metal were ground together, pressed into pellets and heated in air for 30 mins at 1000°C , in a platinum crucible. Due to evaporation of OsO_4 , additional amounts of Os (10% mol) were added. The sample was reground and re-pressed into a pellet than heated for an additional 30 mins at 1000°C in air. This process was repeated once more but finally heated for 24 hr at 1000°C and a phase-pure sample was obtained.

2.2. X-Ray Diffraction

Room temperature powder X-ray diffraction data were obtained on a PANalytical XPert Pro diffractometer with an XCelerator detector. $\text{Cu-K}\alpha_1$ radiation ($\lambda = 1.54056 \text{ \AA}$) with 2θ step interval of 0.0167° was used for data collection. Rietveld refinements were performed using the FullProf suite [25].

2.3. Neutron Diffraction

Neutron powder diffraction data were collected at the Canadian Neutron Beam Centre, Chalk River Nuclear Laboratories, using the C2 diffractometer with neutron wavelengths of 1.3305 \AA and 2.3719 \AA at temperatures of 280 K and 4 K.

2.4. Magnetic Susceptibility

A Quantum Design MPMS SQUID Magnetometer was used to perform bulk magnetization measurements. The magnetic susceptibility measurements were collected from 2 K to 300 K with applied field of 1000 Oe (0.10 T). Isothermal magnetization measurements were collected at 2, 25, and 100 K, from -5 to 5 T.

2.5. Muon Spin Relaxation

Muon spin relaxation (μSR) data were collected in time-differential (TD) mode using the LAMPF spectrometer at the M20 surface muon beamline at TRIUMF, Vancouver,

Canada. μSR measurements serve as a probe of local magnetism, employing the fact that muons possess a sizable magnetic dipole moment. A beam of initially 100% spin-polarized positive muons (μ^+) is produced, and muons are implanted one at a time into the sample. Each muon comes to rest, typically at a crystallographic interstitial site or near an oxygen anion. The muon then undergoes Larmor precession in the local field at the muon site, with a frequency $f = \gamma B$, with $\gamma = 135.5 \text{ MHz/T}$, until it decays (with a characteristic $2.2 \mu\text{s}$ timescale). The muon then emits a positron, preferentially along the instantaneous spin axis at the time of decay. These emitted positrons are detected by a pair of detectors positioned around the sample (often in front of, F, and behind, B, the sample) and the decay asymmetry is calculated as

$$\text{Asy} = (B - F)/(B + F) \quad (2)$$

The time dependence of this decay asymmetry follows that of the muon spin polarization $G_z(t)$, and from this the internal local field distribution may be deduced. Measurements performed in zero applied field are sensitive to extremely small internal magnetic fields (on the order of 1 G), including those due to nuclear magnetic moments, as well as magnetic fields which arise from the slowing down and static ordering of electronic moments. Measurements taken in a weak applied transverse field (wTF) are used to calibrate the initial and baseline decay asymmetries, to account for detector efficiencies and areas.

A continuous beam of spin-polarized muons was implanted into a $\sim 1 \text{ g}$ powder sample loaded into a ^4He cryostat, and two-counter muon spin decay asymmetries were collected from 0 to $10 \mu\text{s}$ at temperatures ranging from 2 K up to 130 K. Measurements were taken in zero field (ZF) and weak transverse field (wTF) modes using the ultra-low background sample holder.

3. Results and Discussion

3.1. Crystal Structure

Rietveld refinement of both powder x-ray and neutron diffraction data at 280 K confirmed the cubic $Fm\bar{3}m$ structure, in accordance with the previously reported x-ray diffraction data [24]. The results pertaining to lattice constants, positional and displacement parameters, and goodness of fit are shown in Table II. Figure 2 shows the results of the refinement at 3.5 K. The results from the refinement indicate that, to within the resolution of the data, the phase retains cubic symmetry at 3.5 K with $a = 8.3462(7) \text{ \AA}$. Simulations of plausible $I4/m$ models indicate that a tetragonal distortion as small as $c/a = 1.004$ would have been easily detected. This is consistent with previous reports that $Fm\bar{3}m$ symmetry is retained to 17 K from x-ray diffraction data [24]. No evidence for B-site (Ca/Os) disorder was found. This is consistent with earlier reports of $<3\%$ B-site disorder in similar double perovskites (*e.g.* [7, 10, 15]), and the large difference in valence and ionic radius between Ca^{2+} and Os^{6+} solidly places $\text{Ba}_2\text{CaOsO}_6$ in the "rock salt ordered" region of the phase diagram of Anderson *et al.* [1].

3.2. Magnetic Susceptibility

In Figure 3 we show d.c. susceptibility data for the $\text{Ba}_2\text{CaOsO}_6$ sample studied here. The inset shows a fit to the Curie-Weiss law for $T > 100 \text{ K}$ which yields C

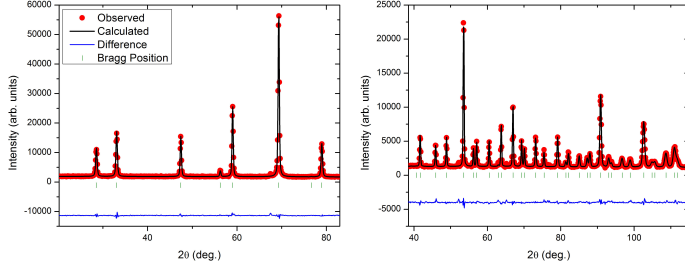


Figure 2. Low-temperature (3.5 K) powder neutron diffraction patterns of $\text{Ba}_2\text{CaOsO}_6$, measured with neutron wavelengths (a) $\lambda = 2.3719 \text{ \AA}$ and (b) $\lambda = 1.3305 \text{ \AA}$.

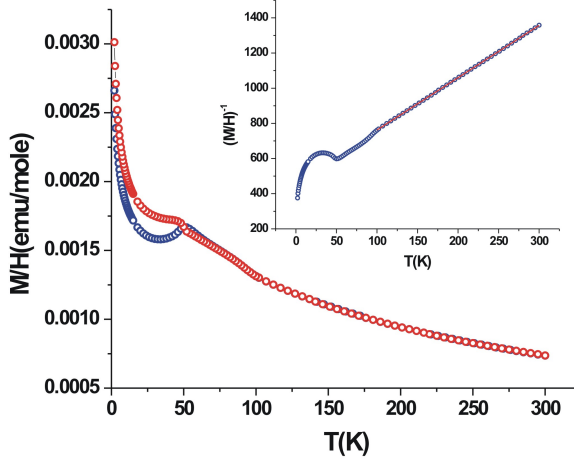


Figure 3. d.c. susceptibility data for $\text{Ba}_2\text{CaOsO}_6$. Field cooled curve (FC, red) and Zero-field cooled curve (ZFC, blue). The inset shows the inverse susceptibility data fitted to the Curie-Weiss law (red line) yielding the constants given in the text.

$= 0.3361(3) \text{ emu-K/mole}$ [$\mu_{\text{eff}} = 1.640(1) \mu_{\text{B}}$], which is much smaller than the spin-only value of 1.00 emu-K/mole [$2.83 \mu_{\text{B}}$], indicating a large influence for SOC, and $\Theta_{\text{CW}} = -156.2(3) \text{ K}$. These results are nearly identical to those reported earlier [24]. Figure 4 shows the low-temperature ZFC data upon which is superimposed Fisher's heat capacity $d(\chi T)/dT$ vs. T , which is expected to exhibit similar variation to the magnetic contribution to the specific heat [26], indicating a likely magnetic phase transition between 47 K and 50 K.

The field dependence of the magnetization is shown in Figure 5 at 100 K, 25 K and 2 K. While linear behaviour with negligible hysteresis is seen for the two higher temperatures, the 2 K data indicate a small hysteresis and non-linearity.

These results should be contrasted with those for Ba_2YReO_6 , where the Curie-Weiss constants are $\mu_{\text{eff}} = 2.105 \mu_{\text{B}}$ and $\Theta_{\text{CW}} = -616(7) \text{ K}$ [10]. While μ_{eff} is significantly closer to the spin-only value of $2.83 \mu_{\text{B}}$, indicating a smaller SOC influence, Θ_{CW} is four times larger, a remarkable result which indicates a much greater

Table 2. The results from the Rietveld refinement of powder neutron data for Ba_2CaOsO_6 in $Fm\bar{3}m$ at 280 K. The refinement was done simultaneously with two wavelengths from neutrons and one from x-ray ($\lambda = 1.541$ Å). Included are selected interatomic distances for Ba_2CaOsO_6 at 280 K. Refinement results at 3.5 K, done simultaneously with two wavelengths from neutrons only, are reported in square brackets [] below the 280 K data.

	280 K [3.5 K]			
	x	y	z	B_{iso} (Å ²)
Ba	0.25	0.25	0.25	0.587(52) [0.024(37)]
Ca	0.5	0.5	0.5	0.704(105) [0.193(85)]
Os	0	0	0	0.269(57) [0.25]
O	0.2294(23) [0.22911(16)]	0	0	0.966(50) 0.412(33)]
a	8.3619(6) [8.3462(7)]			
<hr/>				
	$\lambda =$	1.33 Å	2.37 Å	1.541 Å
χ^2		2.91 [4.16]	1.98 [4.19]	2.78
R_p		3.56 [2.74]	3.69 [2.74]	13.8
R_{wp}		4.72 [3.84]	5.07 [3.85]	17.7
R_{exp}		2.77 [1.88]	3.6 [1.88]	10.61
R_{Bragg}		3.69 [3.23]	2.2 [1.20]	15.2
R_F		2.26 [2.12]	1.68 [0.76]	12.3
<hr/>				
Bond (Å)	Ba–O	2.9613(2) [2.9561(8)]		
	Ca–O	2.2619(17) [2.2610(6)]		
	Os–O	1.9191(17) [1.9123(3)]		

net antiferromagnetic exchange and, subsequently, a much more significant role for geometric frustration. The low-temperature susceptibility data for Ba_2YReO_6 also show more complex behaviour with two rather broad maxima at 25 K and 50 K. Heat

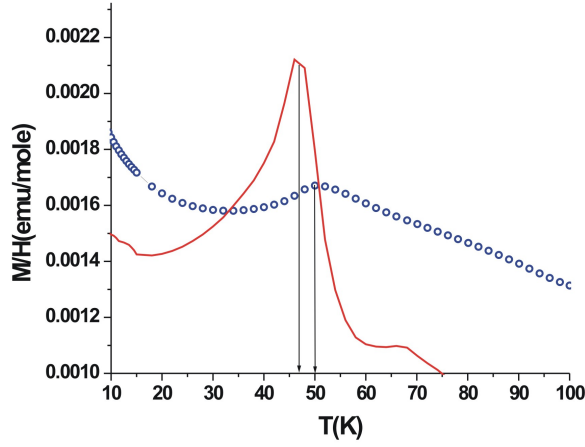


Figure 4. Low temperature ZFC data (blue) for Ba_2CaOsO_6 . Superimposed is a plot of the Fisher heat capacity $d(\chi T)/dT$ vs. T (solid red line), which can be expected to scale as the magnetic contribution to the heat capacity [26], indicating a magnetic phase transition between 47 and 50 K.

capacity data show two broad maxima at the same temperatures, which is not generally indicative of long-range order (more typically indicated by a λ -type anomaly); for example, the spin glasses Sr_2CaReO_6 [22] and Sr_2MgReO_6 [23] both exhibit broad heat capacity anomalies.

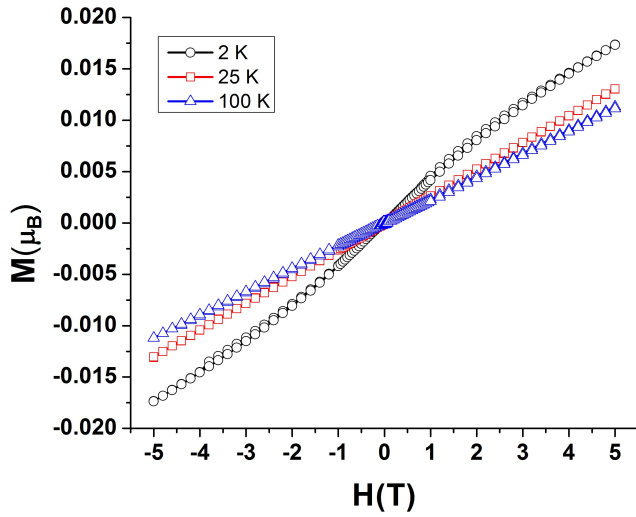


Figure 5. Hysteresis loops for Ba_2CaOsO_6 at 2, 25 and 100 K.

3.3. Magnetic Neutron Diffraction

Figure 6 shows the 280 K and 4 K neutron diffraction patterns along with the difference intensity. Even with very long counting times, 63 hours at 3.5 K, no evidence for magnetic reflections was found between 10 and 85 degrees 2Θ . As a small ordered moment is expected, simulations were carried out assuming a Type I f.c.c. magnetic structure as found for Ba_2YRuO_6 for a range of ordered moments on the Os site [8]. For moments lower than $0.7 \mu_B/\text{Os}$ the ratio $(100)_{\text{mag}}/(111)_{\text{nucl}}$ falls below 1% and this is assigned as the likely upper limit of a detectable moment. In another approach, using the same instrument under the same experimental conditions, a moment of $0.3 \mu_B/\text{Ti}^{3+}$ ion was detected in the perovskite NdTiO_3 [27]. Taking into account the unit cell volume (243 \AA^3) and the number of magnetic ions per unit cell (4) a moment density of $\sim 5 \times 10^{-3} \mu_B/\text{\AA}^3$ is estimated as the upper limit. For Ba_2CaOsO_6 (cell volume 581 \AA^3) similar considerations also suggest a moment limit of $\sim 0.7 \mu_B/\text{Os}$ ($\sim 5 \times 10^{-3} \mu_B/\text{\AA}^3$). Thus, it is possible to state with reasonable confidence that any ordered moment on Os^{6+} , assuming Type I f.c.c. long range order, must be less than $0.7 \mu_B$.

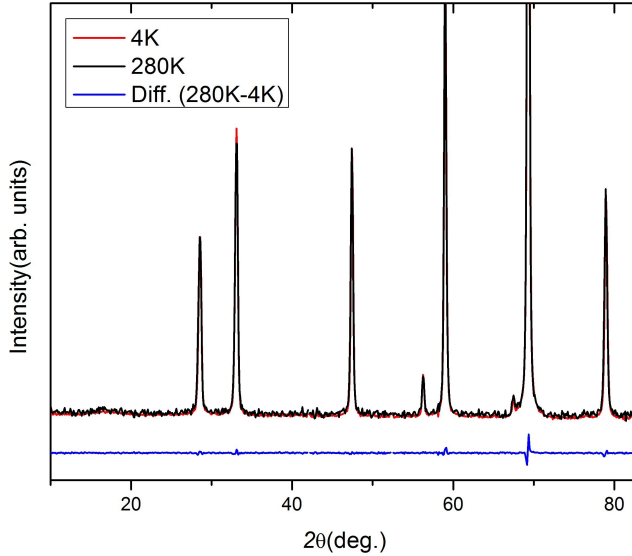


Figure 6. Neutron diffraction patterns at 4 K and 280 K, along with the difference between the two patterns. The counting time for the 4 K data was 63 hr. Arrows indicate the locations of the $[100]$ and $[110]$ magnetic Bragg reflections, as expected for Type I f.c.c. antiferromagnetic order; no intensity differences at these or any other locations are seen.

3.4. Muon Spin Relaxation

Our ZF- μ SR spectra very clearly show the onset of rapid relaxation and precession below 50 K, as seen in Figure 7. By base temperature, a clear and long-lived precessing asymmetry persists to at least $4 \mu\text{s}$, with a frequency of 0.81 MHz.

The entire muon spin precession signal is fit to a sum of precessing and relaxing

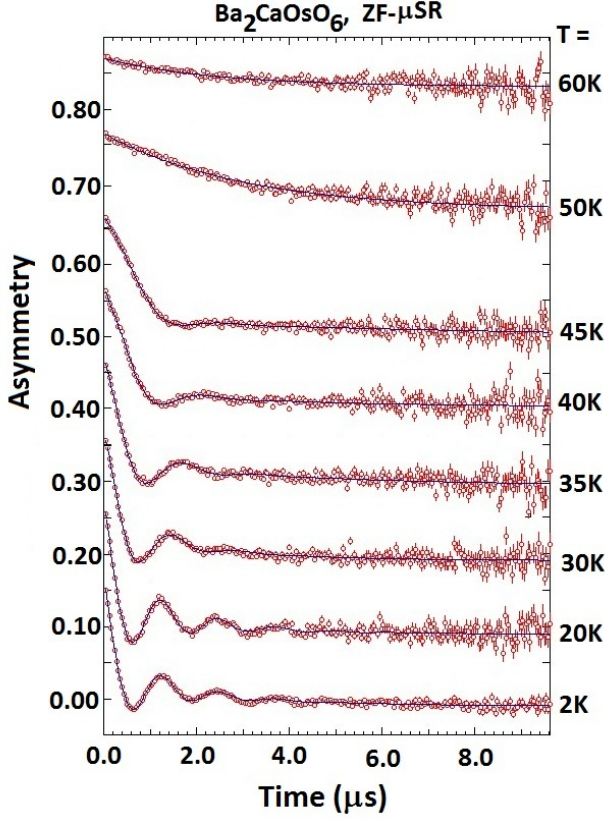


Figure 7. Zero-Field (ZF) muon spin relaxation data, fit to the function in Eq. 3. Rapid relaxation and muon spin precession are visible below the ordering temperature 50 K; the existence of long-lived precession at low temperatures is indicative of long-range order. The vertical axis depicts raw asymmetry, with offsets of 0.1 added to separate the traces.

asymmetries:

$$Asy(t) = A_1 e^{(-\lambda_1 t)} \cos(2\pi f t) + A_2 e^{(-\lambda_2 t)} + A_3 e^{(-\lambda_3 t)} \quad (3)$$

In this fit function, the first two terms correspond to rapid precessing and non-precessing relaxing asymmetries present below the ordering temperature, whereas the third term corresponds to a slow relaxation seen at all temperatures. Figure 8 shows the temperature dependence of the precession frequency $f(T)$, fit to a power-law temperature dependence

$$f(T) = f_0 (1 - (T/T_C))^\beta \quad (4)$$

over the range $30 \text{ K} < T < 50 \text{ K}$ with an exponent β fixed to the Heisenberg value 0.362, yielding $T_C = 48.4 \text{ K}$. There are not enough data points to clearly distinguish between Ising, XY and Heisenberg critical exponent values. The three relaxation rates λ_1 , λ_2 and λ_3 are depicted in Figure 9; due to interplay between the three terms, particularly near the ordering temperature, a total relaxation $\lambda_T = \lambda_1 + \lambda_2 + \lambda_3$ is also plotted. Near base temperature, the fast non-precessing relaxation rate λ_2 flattens

out at approximately $6.5 \mu s^{-1}$, while the precessing relaxation rate λ_1 levels out at $1 \mu s^{-1}$. The slow relaxation rate λ_3 remains at around 0.3 to $0.4 \mu s^{-1}$ throughout the ordered region. Note that these results (Fig. 8) are consistent with a continuous phase transition.

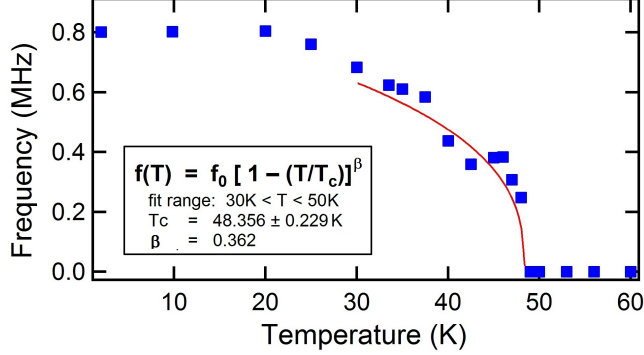


Figure 8. Muon spin precession frequency f as a function of temperature. The precessing signal abruptly becomes visible below the ordering temperature, and the frequency has been fit over the temperature range $30 \text{ K} < T < 50 \text{ K}$ to a power-law dependence $f(T) = f_0(1 - T/T_C)^\beta$, with $T_C = 48.4 \text{ K}$ and β fixed to the Heisenberg value of 0.362.

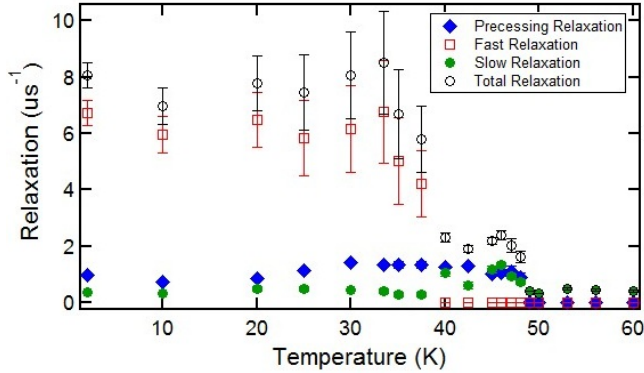


Figure 9. Muon spin relaxation rates λ_1 (precessing), λ_2 (fast) and λ_3 (slow) as described by the fit function in Eq. (2). Due to interplay between the terms near the ordering temperature, a total relaxation λ_T , defined as the sum of the three individual relaxation rates, is also plotted.

Such long-lived muon spin precession is associated with a highly homogeneous field distribution at the muon site, with $f = \gamma B$, with the muon gyromagnetic ratio $\gamma = 135.5 \text{ MHz/T}$, corresponding to an internal field at the muon site of 60 G.

Muon spin relaxation data were collected under identical conditions for the antiferromagnetically long-range ordered isostructural material Ba_2YRuO_6 ($Ru^{5+} 4d^3$), known to exhibit an ordered moment size of $2.2 \mu_B$, as shown in Figure 10. In this material, a similar relaxation function was used, although the precessing frequency reached 45.5 MHz at base temperature (with evidence for a second precessing frequency of 25-27 MHz), corresponding to an internal field at the muon site of 3.35 kG,

a factor 57 times larger than in $\text{Ba}_2\text{CaOsO}_6$. However, the relaxation rates λ_1 and λ_2 reach values of about $10 \mu\text{s}^{-1}$ and $65.5 \mu\text{s}^{-1}$ at $T = 2 \text{ K}$, only a factor of 10 higher than in $\text{Ba}_2\text{CaOsO}_6$.

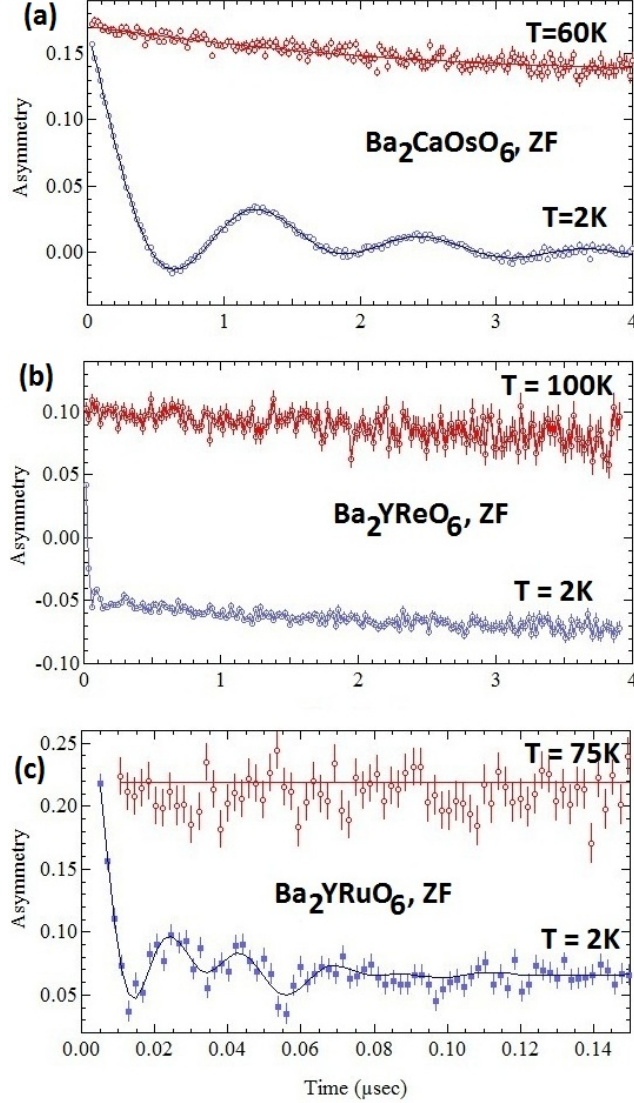


Figure 10. Comparison of ZF- μ SR data for the isostructural systems $\text{Ba}_2\text{CaOsO}_6$ (a), Ba_2YReO_6 (b) and Ba_2YRuO_6 (c). Note the much shorter timescale in the Ba_2YRuO_6 panel. Ba_2YRuO_6 , known to exhibit commensurate long-range antiferromagnetic order, and $\text{Ba}_2\text{CaOsO}_6$ both exhibit clear precession of muon spins, corresponding to a relatively homogeneous and static internal field, indicative of long-range magnetic order. Ba_2YReO_6 , in contrast, exhibits rapid relaxation without sustained precession characteristic of a frozen but spatially disordered ground state.

Previously, muon spin relaxation data have been reported on the isostructural and isoelectronic material Ba_2YReO_6 ($\text{Re}^{5+} 5d^2$), which is known to exhibit a

glassy ground state [10], also shown in Figure 10. In contrast to Ba_2YRuO_6 and $\text{Ba}_2\text{CaOsO}_6$, Ba_2YReO_6 exhibits only rapid relaxation with a single half-oscillation at low temperatures, as expected for a static glassy system [28], with no evidence for sustained precessing behaviour. We therefore determine that $\text{Ba}_2\text{CaOsO}_6$, like Ba_2YRuO_6 and unlike Ba_2YReO_6 , exhibits long-range order below its ordering temperature $T_C = 50$ K which is of course consistent with susceptibility and heat capacity data.

Further, since muon spin precession and relaxation rates scale linearly with the internal field, we determine that the internal field strengths in $\text{Ba}_2\text{CaOsO}_6$ are at least a factor of 10 times weaker than in Ba_2YRuO_6 . If the ordered moment distribution in the two is identical, we may determine an upper limit on the ordered moment size in $\text{Ba}_2\text{CaOsO}_6$ of $0.2 \mu_B$, based on the $2.2 \mu_B$ ordered moment in Ba_2YRuO_6 [8]. However, μSR is a local probe of magnetism so the spatial range of the magnetic order in $\text{Ba}_2\text{CaOsO}_6$ cannot be determined independently by this method. Indeed, muon spin precession has been seen in materials exhibiting short-range magnetic order [29], provided that the ordering correlation lengths are long relative to the spatial scale accessible to the muon. Nonetheless, as has been emphasized, heat capacity and susceptibility data clearly establish long range order in this material. Note that the estimated ordered moment size of $0.2 \mu_B$ per Os^{6+} is consistent with similar moment sizes seen in other double perovskite antiferromagnets such as $\text{Ba}_2\text{NaOsO}_6$ [12]. For such small ordered moments, essentially undetectable to neutron powder diffraction, μSR provides nearly the only means of measurement. In particular, magnetic Bragg peaks are expected to scale quadratically with the ordered moment size; an ordered moment of $0.2 \mu_B$ would yield a Bragg peak 12 times smaller than the $0.7 \mu_B$ upper limit derived from 63 hr of neutron data.

It is also intriguing that both Ba_2YRuO_6 and Ba_2YReO_6 exhibit significantly higher frustration indices f than $\text{Ba}_2\text{CaOsO}_6$, indicating an increased level of frustration in the former materials. This is particularly intriguing in the case of the rhenate since in addition to being identical in structure, Re^{5+} and Os^{6+} are isoelectronic and, being neighbors on the periodic table, should have a very similar spin-orbit coupling parameter λ , which scales as Z^4 .

3.5. Comparison with Theory

Recently, a mean field theory of ordered cubic double perovskites based on d^2 ions under strong SOC has been published [5]. A rather complex phase diagram is found with seven potential ground states which is reproduced as Figure 11. The y-axis depicts J'/J , where J' is a nearest-neighbor FM interaction scaled to a $J = 1$ AFM nearest-neighbor interaction. The x-axis depicts V/J , which is the similarly normalized quadrupolar interaction defined as

$$V = (9/2)Q^2/a^5 \quad (5)$$

where Q is the quadrupole moment and a is the unit cell constant. This is a repulsive term involving d orbitals on nearest-neighbor sites and Q increases as a function of the degree of hybridization of oxygen p - and metal d -orbitals. Of the seven states, three are ferromagnetic: FM110, FM111 and *. There are also three antiferromagnetic states: AFM100, Δ , and $\bar{\Delta}$; the latter two represent complex four-sublattice structures. The final state is a quadrupolar state, also described as a spin nematic, which does not break time reversal symmetry.

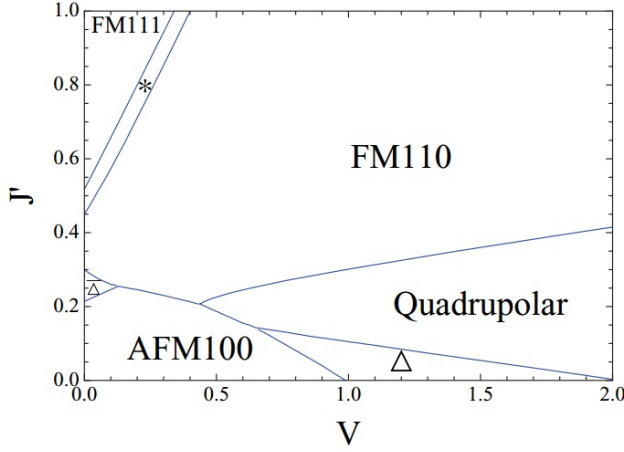


Figure 11. Calculated phase diagram of d^2 double perovskites exhibiting spin-orbit coupling (SOC), under the model Hamiltonian $H = H_{AFM} + H_{FM} + H_{quad}$. The axes represent J' , a nearest-neighbor FM interaction, and V , the quadrupolar interaction defined in the text. Both are normalized by J , representing the nearest-neighbor AFM interaction. Reproduced from Figure 1 in Ref. [5]; copyright (2011) by the American Physical Society.

It is of interest of course to determine the relative placement of $\text{Ba}_2\text{CaOsO}_6$ and Ba_2YReO_6 within this diagram, *i.e.*, with respect to the J'/J and V/J axes. Comparing the Curie-Weiss temperatures, both are strongly negative but $\Theta_{(\text{Ba}_2\text{YReO}_6)}/\Theta_{(\text{Ba}_2\text{CaOsO}_6)} \sim 4$, indicating that $J'/J_{(\text{Ba}_2\text{YReO}_6)} < J'/J_{(\text{Ba}_2\text{CaOsO}_6)}$. To determine the relative V/J positions, the Re–O and Os–O distances should reflect the degree of hybridization with oxygen. These are $1.955(1) \text{ \AA}$ and $1.919(2) \text{ \AA}$, respectively, indicating a larger V/J for the $\text{Ba}_2\text{CaOsO}_6$ phase. With the present work and previous heat capacity studies [24] the ground state of the CaOs material is well established as AFM and limits can be placed on the magnitude of the ordered Os^{6+} moment using both neutron diffraction and μSR results. Unfortunately, the type of AFM order cannot yet be determined due to the very small ordered moment. $\text{Ba}_2\text{CaOsO}_6$ is thus described by the small J'/J part of Figure 11, and the likely choices are AFM100, Δ or $\bar{\Delta}$, the latter two being complex four-sublattice states.

There is one further important result from Ref. [5] which can guide this choice. The calculations were also carried out for $T > 0$ and thus include predictions concerning the nature of the phase transitions from the high temperature paramagnetic state to any of the $T = 0$ phases of Fig. 11. The transitions to Δ and $\bar{\Delta}$ are found to be continuous while that to AFM100 is strongly first order. The μSR data of Fig. 8 indicate a continuous transition for $\text{Ba}_2\text{CaOsO}_6$ and thus there is a strong argument for either the Δ or $\bar{\Delta}$ ground states. Indeed, it was suggested that $\text{Ba}_2\text{CaOsO}_6$ might be assigned to $\bar{\Delta}$. In the same paper it was postulated that Ba_2YReO_6 could be a candidate for the quadrupolar-spin nematic region of the phase diagram. However, this seems inconsistent, if $V(\text{Ba}_2\text{CaOsO}_6) > V(\text{Ba}_2\text{YReO}_6)$, as argued here. For any of the above choices of ground state for $\text{Ba}_2\text{CaOsO}_6$, given that both V/J and J'/J are smaller for Ba_2YReO_6 , the AFM100 state would be expected for this material, according to Fig. 11. It was suggested that disorder precludes the establishment of one of the predicted ground states for Ba_2YReO_6 . However, the

level of one type of potential disorder, namely Y/Re intersite exchange, was examined using the very sensitive technique of ^{89}Y magic angle spinning (MAS) NMR and such disorder was not detected, placing an upper limit of $\lesssim 0.5\%$ on B/B' site disorder [10]. Interestingly, Y/M site disorder was easily seen by this method in the closely related double perovskites, Ba_2YMO_6 at the levels of 1% ($\text{M} = \text{Ru}$) and 3% ($\text{M} = \text{Mo}$) [7, 15]. The ground states of these two materials appear to be unaffected by such larger disorder levels, as seen in Table I. That an ordered ground state is not found for Ba_2YReO_6 indicates either that a very low, as yet undetectable, disorder level plays a decisive role or that one must go beyond the mean theory level of Ref. [5] to find an explanation.

4. Conclusions

The double perovskite $\text{Ba}_2\text{CaOsO}_6$, based on the $5d^2$ ion, Os^{6+} , has been synthesized and characterized using neutron diffraction and μSR techniques which complement earlier studies of the heat capacity and magnetic susceptibility [24]. It is now clear that cubic $Fm\bar{3}m$ symmetry is retained to 3.5 K and that the material orders antiferromagnetically near 50 K with an estimated ordered moment size of $\sim 0.2\mu_B$. However, the long-range nature of the ordered state cannot be determined solely from the μSR data, as μSR is a local probe sensitive only to local field environments. This behaviour is in remarkable contrast to that of its isostructural and isoelectronic doppelganger, Ba_2YReO_6 , which, with essentially the same cubic unit cell constant, has a Θ_{CW} four times larger and is found in a spin frozen ground state with $T_g \sim 35$ K [10]. The behaviour of $\text{Ba}_2\text{CaOsO}_6$ can also be contrasted with the closely related $4d^3$ and $4d^1$ based double perovskites, Ba_2YRuO_6 and Ba_2YMoO_6 , which also exhibit cubic $Fm\bar{3}m$ symmetry and have AFM [7, 8] and gapped spin singlet ground states [14, 15, 16] respectively. This is consistent of a general evolution from ordered to increasingly disordered ground states as one proceeds from d^3 to d^2 to d^1 systems. As monoclinic $\text{La}_2\text{LiReO}_6$ also does not order [10], $\text{Ba}_2\text{CaOsO}_6$ is the first $5d^2$ based double perovskite which does, exhibiting μSR spectra more closely resembling the $4d^3$ Ba_2YRuO_6 than the isoelectronic $5d^2$ system Ba_2YReO_6 .

The properties of $\text{Ba}_2\text{CaOsO}_6$ and Ba_2YReO_6 have been discussed in the context of a recently published mean field theory for nd^2 double perovskites under the influence of strong SOC [5]. While $\text{Ba}_2\text{CaOsO}_6$ might be described in terms of an exotic four sublattice AFM state, Δ or $\bar{\Delta}$, it is difficult to accommodate Ba_2YReO_6 within this theoretical framework. While some level of disorder might play a role in the latter case, there is scant experimental evidence.

Acknowledgments

J.E.G. thanks the Natural Sciences and Engineering Research Council of Canada (NSERC) for support through the Discovery Grant program, and Dr. E. Kermarrec for useful discussions. G. M. L. acknowledges support from NSERC. The Columbia group has been supported by US NSF under DMR-1105961 and OISE-0968226 (PIRE: Partnership for International Research and Education) and by JAEA (Japan) under the REIMEI project. S. C. acknowledges travel support from the Friends of Todai Foundation. We thank the TRIUMF CMMS staff for invaluable technical assistance with μSR experiments.

References

- [1] M. T. Anderson and K. B. Greenwood and G. A. Taylor and K. R. Poppelmeier. *Prog. Solid St. Chem.*, 22:197–233, 1993.
- [2] V. M. Goldschmidt. *Die Naturwissenschaften*, 14:477, 1926.
- [3] C. J. Howard and B. J. Kennedy and P. M. Woodward. *Acta. Cryst. B*, 59:463–471, 2003.
- [4] G. Chen and R. Pereira and L. Balents. *Phys. Rev. B*, 82:174440, 2010.
- [5] G. Chen and L. Balents. *Phys. Rev. B*, 84:094420, 2011.
- [6] T. Dodds and T.-P. Choy and Y. B. Kim. *Phys. Rev. B*, 84:104439, 2011.
- [7] T. Aharen and J. E. Greedan and F. Ning and T. Imai and V. Michaelis and S. Kroeker and H. Zhou and C. R. Wiebe and L. M. D. Cranswick. *Phys. Rev. B*, 80:134423, 2009.
- [8] J. P. Carlo and J. P. Clancy and K. Fritsch and C. A. Marjerrison and G. E. Granroth and J. E. Greedan and H. A. Dabkowska and B. D. Gaulin. *Phys. Rev. B*, 88:024418, 2013.
- [9] D. Iwanaga and Y. Inaguma and M. Itoh. *Mat. Res. Bull.*, 35:449–457, 2000.
- [10] T. Aharen and J. E. Greedan and C. A. Bridges and A. A. Aczel and J. A. Rodriguez and G. J. MacDougall and G. M. Luke and V. K. Michaelis and S. Kroeker and C. R. Wiebe and H. Zhou and L. M. D. Cranswick. *Phys. Rev. B*, 81:064436, 2010.
- [11] K. E. Stitzer and M. D. Smith and H.-C. zur Loye. *Solid State Sciences*, 4:311, 2002.
- [12] A. S. Erickson and S. Misra and G. J. Miller and R. R. Gupta and Z. Schlesinger and W. A. Harrison and J. M. Kim and I. R. Fisher. *Phys. Rev. Lett.*, 99:016404, 2007.
- [13] A. J. Steele and P. J. Baker and T. Lancaster and F. L. Pratt and I. Franke and S. Ghannadzadeh and P. A. Goddard and W. Hayes and D. Prabhakaran and S. J. Blundell. *Phys. Rev. B*, 84:144416, 2011.
- [14] M. A. de Vries and A. C. McLaughlin and J.-W. G. Bos. *Phys. Rev. Lett.*, 104:177202, 2010.
- [15] T. Aharen and J. E. Greedan and C. A. Bridges and A. A. Aczel and J. A. Rodriguez and G. J. MacDougall and G. M. Luke and T. Imai and V. K. Michaelis and S. Kroeker and H. Zhou and C. R. Wiebe and L. M. D. Cranswick. *Phys. Rev. B*, 81:224409, 2010.
- [16] J. P. Carlo and J. P. Clancy and T. Aharen and Z. Yamani and J. P. C. Ruff and J. J. Wagman and G. J. Van Gastel and H. M. L. Noad and G. E. Granroth and J. E. Greedan and H. A. Dabkowska and B. D. Gaulin. *Phys. Rev. B*, 84:100404(R), 2011.
- [17] C. P. Khattak and D. E. Cox and F. F. Y. Wang. *J. Solid State Chem.*, 17:323–325, 1976.
- [18] A. K. Azad and S. A. Ivanov and S.-G. Eriksson and J. E. Eriksen and H. Rundlöf and R. Mathew and P. Svedlindh. *J. Magn. Magn. Mater.*, 237:124, 2001.
- [19] A. Muñoz and J. A. Alonso and M. T. Casais and M. J. Martinez-Lope and M. T. Fernandez-Diaz. *J. Phys.: Condens. Matter.*, 14:8817, 2002.
- [20] A. A. Aczel and D. E. Bugaris and L. Li and J.-Q. Yan and C. de la Cruz and H. C. zur Loye and S. E. Nagler. *Phys. Rev. B*, 87:014435, 2013.
- [21] A. A. Aczel and P. J. Baker and D. E. Bugaris and J. Yeon and H.-C. zur Loye and T. Guidi and D. T. Adroja. *Phys. Rev. Lett.*, 112:117603, 2014.
- [22] C. R. Wiebe and J. E. Greedan and G. M. Luke and J. S. Gardner. *Phys. Rev. B*, 65:144413, 2002.
- [23] C. R. Wiebe and J. E. Greedan and P. P. Kyriakou and G. M. Luke and J. S. Gardner and A. Fukaya and I. M. Gat-Malureanu and P. L. Russo and A. T. Savici and Y. J. Uemura. *Phys. Rev. B*, 68:134410, 2003.
- [24] K. Yamamura and M. Wakeshima and Y. Hinatsu. *J. Solid State Chem.*, 179:605–612, 2006.
- [25] J. Rodriguez-Carvajal. *Physica B*, 192:55–69, 1993.
- [26] M. E. Fisher. *Philos. Mag.*, 7:1731, 1962.
- [27] A. S. Sefat and J. E. Greedan and L. M. D. Cranswick. *Phys. Rev. B*, 74:104418, 2006.
- [28] Y. J. Uemura and T. Yamazaki and D. R. Harshman and M. Denba and E. J. Ansaldo. *Phys. Rev. B*, 31:546–563, 1985.
- [29] C. R. Wiebe and P. L. Russo and A. T. Savici and Y. J. Uemura and G. J. MacDougall and G. M. Luke and S. Kuchta and J. E. Greedan. *J. Phys.: Condens. Matter*, 17:6469, 2005.